Modelling of rooms with active chilled beams

Citation for the original published paper (version of record):
Filipsson, P., Trüschel, A., Gräslund, J. et al (2020). Modelling of rooms with active chilled beams. Journal of Building Performance Simulation, 13(4): 409-418.
http://dx.doi.org/10.1080/19401493.2020.1752801

Journal of Building Performance Simulation

ISSN: 1940-1493 (Print) 1940-1507 (Online) Journal homepage: https://www.tandfonline.com/loi/tbps20

Modelling of rooms with active chilled beams

Peter Filipsson, Anders Trüschel, Jonas Gräslund & Jan-Olof Dalenbäck

To cite this article: Peter Filipsson, Anders Trüschel, Jonas Gräslund & Jan-Olof Dalenbäck (2020) Modelling of rooms with active chilled beams, Journal of Building Performance Simulation, 13:4, 409-418, DOI: 10.1080/19401493.2020.1752801

To link to this article: https://doi.org/10.1080/19401493.2020.1752801

Published online: 16 Apr 2020.

JOURNAL OF BUILDING PERFORMANCE SIMULATION
2020, VOL. 13, NO. 4, 409–418
https://doi.org/10.1080/19401493.2020.1752801

Modelling of rooms with active chilled beams

Peter Filipsson [a,b], Anders Trüschel[a], Jonas Gräslund[a,c] and Jan-Olof Dalenbäck [a]

[a]Division of Building Services Engineering, Department of Architecture and Civil Engineering, Chalmers University of Technology, SE-412 96 Gothenburg, Sweden; [b]CIT Energy Management AB, SE-412 88 Gothenburg, Sweden; [c]Skanska Commercial Development Nordic AB, SE-112 74 Stockholm, Sweden

ABSTRACT

Active chilled beams (ACBs) are often modelled as generic cooling devices. Due to induction, the air flow discharged from an ACB is several times higher than supplied from the air handling unit, and due to its design, it affects the temperature of the ceiling to a greater extent than an arbitrary cooling device. This paper investigates the impact of taking these features into account when simulating air and operative temperature in a room equipped with an ACB. The building performance simulation software IDA ICE is used for analysis and the simulations are compared with full-scale experiments. The main findings are that simulations which take into account the features mentioned above correspond more closely with measurements. If designing for a certain operative temperature, this reduces the required design cooling capacity. Although negligible in many applications, the magnitude of this reduction is 9% with high-temperature cooling.

ARTICLE HISTORY
Received 27 November 2019
Accepted 2 April 2020

KEYWORDS
Active chilled beams; induction ratio; CHTC; IDA ICE; measurements

1. Introduction

Space Cooling is the fastest growing end-use of energy in buildings. The International Energy Agency recently proclaimed the growth in global demand for space cooling as a blind spot of energy policy and one of the most critical energy issues of our time (IEA 2018). Sustainable space cooling technologies are required in order to meet the ever-growing demand without further worsening the situation.

1.1. Active chilled beams

One example of energy efficient technology for space cooling is the use of active chilled beams (ACB). The operation of the most common type of ACB is illustrated in Figure 1.

Primary air is provided from an air handling unit while chilled water is circulated through a cooling coil inside the ACB. The primary air enters the room via a pressure plenum and several nozzles along the beam. The high primary air velocity generated by the nozzles induces secondary air (room air) that cools down as it passes the coil. The mixed air is then discharged into the room through slots along both long sides of the beam and flows attached to the ceiling by means of the Coandă effect. Proper dimensioning should ensure no separation of the supply air plane jet from the ceiling (Cao et al. 2008).

The secondary air flow rate divided by the primary air flow rate is referred to as the induction ratio (IR). A high IR is essential in order to achieve a high cooling capacity. The flow of chilled water is usually controlled as a function of the room air temperature in order to match the cooling capacity with the actual demand.

A key opportunity with ACBs is utilization of high-temperature cooling. In this paper, high-temperature cooling refers to a chilled water supply temperature of ≥ 20°C. This provides major benefits such as increased use of free cooling, efficient operation of chillers, reduced latent load, reduced risk of condensation, reduced thermal losses in the chilled water distribution system and, due to self-regulation, less need for individual room control (Maccarini et al. 2017). Higher chilled water temperature and supply air temperature are also beneficial for the IR (Filipsson et al. 2016) and for the supply air plane jet attachment (Wu et al. 2018) respectively. Filipsson et al. (2020) present a high-temperature ACB system in Stockholm, Sweden, with neither chillers nor room thermostats. The water is chilled in boreholes and by preheating incoming outdoor air (when needed). Due to the self-regulating characteristic of high-temperature cooling, there is no individual room control of the chilled water flow rate.

ACBs are unable to provide latent cooling and condensation on the coil surface should be strictly avoided. Usually, a dew point control system makes sure that the chilled water supply temperature is always at least 1.0°C higher than the indoor air dew point. Consequently, latent loads must be handled by the air handling unit and humid climates require supply air temperatures lower than investigated in this study (Kosonen and Tan 2005).

With high-temperature cooling, the cooling capacity is strongly influenced by the room air temperature. This enables self-regulation, but also increases the need for accurate simulation of air temperature when designing the system. Furthermore, the absence of individual room control systems requires

CONTACT Peter Filipsson filipssp@chalmers.se Division of Building Services Engineering, Department of Architecture and Civil Engineering, Chalmers University of Technology, SE-412 96 Gothenburg, Sweden, CIT Energy Management AB, SE-412 88 Gothenburg, Sweden

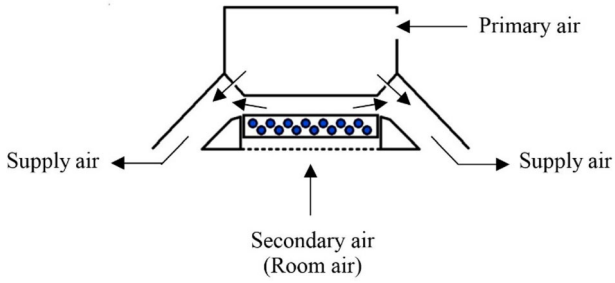

Figure 1. Schematic diagram of an active chilled beam.

more accurate simulation models since safety margins are no longer compensated for by the individual room control.

1.2. Previous work

Several ACB models have been developed during the last couple of years. These range from simple and generic models (CEN 2008) to more sophisticated ones with varying trade-offs between empirics and first principles. Chen et al. (2014) presented a dynamic ACB model with satisfactory accuracy suitable for real-time control and optimization. Maccarini et al. (2015) modelled an active beam used for both heating and cooling using the programming language Modelica. Livchak and Lowell (2012) presented a system of equations describing the operation of active beams (in both heating and cooling mode) and showed that the IR is influenced by the temperatures of water and air due to buoyant forces. Also, Filipsson et al. (2017) captured the effect of air buoyancy when using the NTU method to model the operation of ACBs valid in a wide range of operating conditions including laminar flow of chilled water. Ji et al. (2019) presented a simplified, yet accurate, model further examining the buoyant behaviour and efficiently determined the cooling capacity. Common for all these models is the main focus on cooling capacity (heat transfer) and in that sense, they are considered very accurate. The purpose of determining the IR in these models was mainly to achieve a more accurate determination of the cooling capacity.

Regarding thermal loads and thermal response of building zones, most building performance simulation software is based on the well-established Heat Balance Method (Pedersen, Fisher, and Liesen 1997) which is considered the most accurate cooling load calculation method (Mao, Baltazar, and Haberl 2018).

When incorporating an ACB model in a building performance simulation software, they are often treated as generic and purely convective cooling devices, taking into account neither that the IR influences the internal convective heat transfer nor how the supply air plane jet discharged from the ACB attaches to the ceiling and affects its surface temperature.

Accurate results are obviously dependent on correct input parameters. Domínguez-Muñoz, Cejudo-López, and Carrillo-Andrés (2010) concluded that the convective heat transfer coefficients (CHTC) of internal surfaces in the building zones is one of the most significant sources of uncertainties in cooling load simulations. While radiation and conduction are relatively easy to model by accurately determined parameters (emissivity, conductivity, etc.) convection is influenced by the air movements in the room and thereby more complex.

Heat transfer between room air and the internal surfaces of the room (internal convective heat transfer) is calculated according to the following equation:

$$q''_{conv} = h \cdot (T_{sur} - T_a) \tag{1}$$

where h is the convective heat transfer coefficient (CHTC), T_{sur} is the surface temperature and T_a is the air temperature. In reality, none of the parameters of Equation (1) are uniform across an entire surface (e.g. the floor of a room). In simulations, however, it is assumed that all of them are. As a consequence of the complexity of internal convective heat transfer, numerous CHTC models have been developed. An extensive review was presented by Peeters, Beausoleil-Morrison, and Novoselac (2011). Fisher and Pedersen (1997) performed full-scale experiments and presented correlations between air change rate and CHTCs.

Le Dréau, Heiselberg, and Jensen (2015) performed full-scale experiments to derive CHTCs for rooms equipped with ACBs and radiant walls and concluded that the CHTCs were more accurately calculated as a function of not only the air change rate, but also including the modified Archimedes number.

Adjusted versions of the correlations presented by Fisher and Pedersen (1997) are still used widely in building performance simulation software. These are presented in the following equations:

$$h_{wall} = 0.19 \cdot ACH^{0.8} \tag{2}$$

$$h_{floor} = 0.13 \cdot ACH^{0.8} \tag{3}$$

$$h_{ceiling} = 0.49 \cdot ACH^{0.8} \tag{4}$$

where ACH is the air change rate in the room. These correlations are valid when the reference temperature, T_a in Equation (1), is the supply air temperature. When implemented in building performance simulation software, where fully mixed room air conditions are assumed, Equations (2)–(4) have been reformulated to have the exhaust air temperature as the reference temperature, see the following equations:

$$h_{wall} = 1.208 + 1.012 \cdot ACH^{0.604} \tag{5}$$

$$h_{floor} = 3.873 + 0.082 \cdot ACH^{0.98} \tag{6}$$

$$h_{ceiling} = 2.234 + 4.099 \cdot ACH^{0.503} \tag{7}$$

Equations (5)–(7) are known as the ceiling diffuser model in EnergyPlus (DOE 2010). In IDA ICE (EQUA Simulation AB 2018), the models have been further adjusted to take natural convection into account at low air change rates, see the following equations:

$$h_{wall} = \max\left(1.208 \cdot \frac{\min(5, ACH)}{5} + 1.012 \cdot ACH^{0.604}, f(\Delta T)\right) \tag{8}$$

$$h_{floor} = \max(3.873 \cdot \frac{\min(5, ACH)}{5} + 0.082 \cdot ACH^{0.98}, f((\Delta T)) \tag{9}$$

$$h_{ceiling} = \max\left(2.234 \cdot \frac{\min(5, ACH)}{5} + 4.099 \cdot ACH^{0.503}, f(\Delta T)\right) \tag{10}$$

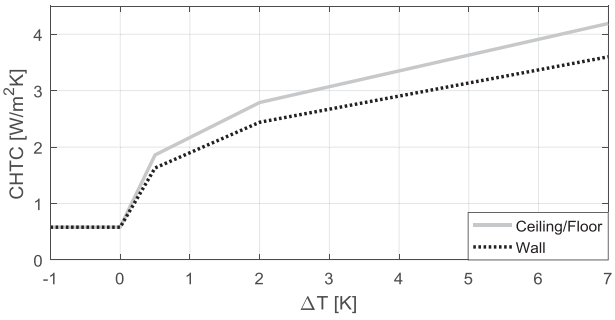

Figure 2. Convective heat transfer coefficient due to natural convection.

where ΔT is the temperature difference between the air and the surface (oppositely for the floor) and $f(\Delta T)$ is known as the BRIS model and presented in Figure 2.

1.3. Objective

An ACB has certain features distinguishing it from many other cooling devices. Of these, the induction of room air (which influences the CHTCs of internal surfaces in the room) and how the air flow discharged from the ACB influences the ceiling surface temperature are often disregarded when modelling ACBs. The objective of the work presented in this paper is to analyse the consequences of taking these features into account when simulating indoor air temperature and operative temperature.

2. Method

The work presented in this paper is based on measurements in a full-scale mockup of an office room and simulations made in the building performance simulation software IDA ICE version 4.8 (EQUA Simulation AB 2018). The description of the method is divided into three parts. The first part deals with the experiments, the second part deals with setting up a model that as much as possible corresponds to the experimental setup and the third part is about a model of a more realistic office room during a whole year.

2.1. Experimental setup

The measurements were carried out in a full-scale mockup of an office room, see Figure 3. The internal dimensions of the room were 3.0 m × 4.2 m × 2.4 m (width × length × height).

The walls were made of 12 mm plasterboard attached on the inside of 100 mm expanded polystyrene. The floor was made of 22 mm fibreboard on top of 6 mm plasterboard and 30 mm expanded polystyrene. The ceiling was a suspended ceiling of 15 mm fibreglass, an air gap of 270 mm under structural lightweight concrete. An electric heater outside of the room was controlled to keep the temperature drop across the walls below 2°C in order to moderate the heat losses from the room. The ACB was positioned in the suspended ceiling in the middle of the room and two thermal dummies (cylindrical cooling load simulators) were positioned in opposite corners of the room. The dummies housed six lightbulbs each and an air gap of 10 cm between the floor and the cylinder and between the cylinder and its cap allowed air flowing through.

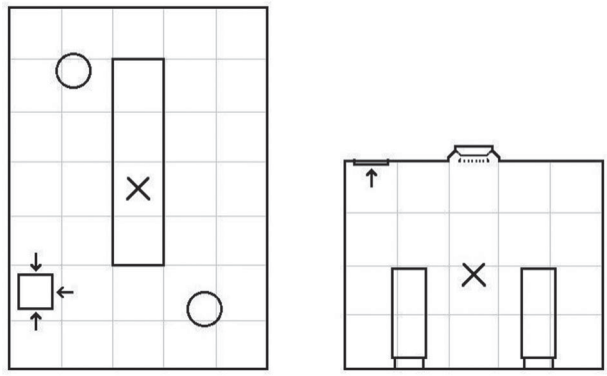

Figure 3. Layout of the room and positions of active chilled beam, exhaust air terminal device and thermal dummies. The X represents the position where room air temperature, globe temperature and air velocity were measured. Top view to the left and front view to the right. Grey lines indicate a distance of 0.6 m.

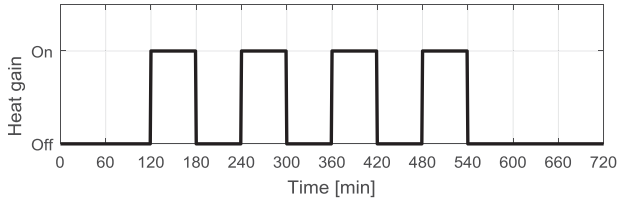

Figure 4. Operation of internal heat gain.

Both the primary air temperature and chilled water supply temperature set-points were kept constant at 20°C. The primary and exhaust air flow set-points were 22.5 l/s (corresponding to the design flow rate of the ACB). The only nonconstant set-point was the internal heat gain which was activated in pulses according to Figure 4.

The flow of chilled water was activated 60 min prior to the heat gain and held constant at 1.78 l/min (corresponding to the design flow rate of the ACB). Two cases were run where the level of internal heat gain was the only differing input, around 58 W/m2 in case 1 and around 38 W/m^2 in case 2.

The experiments were carried out with a Halton CBS active chilled beam with length and width of 2.4 and 0.6 m respectively. The length of the cooling coil was 2.1 m and the primary air plenum design pressure was 100 Pa. At a room air temperature of 25.0°C, chilled water supply temperature of 20.0°C, chilled water flow rate of 1.78 l/min and primary air flow of 22.5 l/s the chilled water cooling power was 379 W. Results obtained from measurements in the laboratory was in accordance with specifications from the manufacturer (±1%). Ceiling attachment of the supply air jet was controlled visually by the use of a smoke pen, but no measurements to quantify the attachment were carried out.

Room air temperature, globe temperature and air velocity were measured in the center of the room at a height of 1.1 m. The purpose of measuring globe temperature and air velocity was to determine the mean radiant temperature in accordance with ISO 7726 (ISO 1998). The operative temperature was approximated as the mean value of air and mean radiant temperature, since this is how IDA ICE approximate operative temperature. The globe temperature was measured (with an uncertainty of ±0.1°C) in a matte black globe with a diameter of 150 mm. Temperatures

of room air, primary air and chilled water were measured with PT100 resistance temperature detectors adjusted with respect to a reference instrument (±0.02°C). Air velocity was measured with an omnidirectional hot-wire anemometer (±0.03 m/s). Flow of chilled water was measured with an ultrasonic flow sensor (±2.25%) and primary air flow was measured with a differential pressure transmitter connected to a measuring damper resulting in a combined uncertainty of ±7%. Specified uncertainty of the measuring damper refers to an average of several damper positions. According to the manufacturer, the uncertainty is lower when fully open, which was the case during the experiments. All uncertainties refer to a coverage factor $k = 2$ and all parameters were sampled with a frequency of one per minute.

2.2. Model description

The model was designed to correspond to the experiments as much as possible. Dimensions and materials of the envelope of the room were set as specified in the previous section. The model comprised three adjacent zones. One representing the core room, one representing the ambient room and one zone representing the air gap between the suspended ceiling and the concrete roof. Measurements of primary air and ambient air temperatures were used as input to the model. The simulations were carried out in the building performance simulation software IDA ICE. Heat transfer by conduction, convection and radiation is calculated for each surface in the room to determine the room air temperature and operative temperature, in accordance with the widely established heat balance method. Validation has been carried out in several research projects, both validation of the heat balance method in general (Chantrasrisalai et al. 2003) and validation of IDA ICE specifically, both by measurements (Loutzenhiser, Manz, and Maxwell 2007) and by intermodel comparison through ANSI/ASHRAE Standard 140-2004 (EQUA Simulation 2010).

2.2.1. Internal heat gain

The measured power of internal heat gain was used as input to the model. However, due to the thermal inertia of the dummies, there was a lag between measured power and emission of heat. This was taken into account by measuring the response time between a step-change in power and the surface temperature of the dummies. The surface temperature reached 63% of its final rise after 5 min. It was assumed that half of the internal heat gain was emitted instantaneously and half of it emitted with a response time equal to the response time of the surface temperature of the dummies. The result of this is presented in Figure 5.

In IDA ICE version 4.8, it is not possible to simulate internal heat gain from cylindrical objects. The dummies were instead modelled as flat electrical radiators attached to the walls. By modelling these radiators with a height of 2.36 m and a width of 0.58 m positioned in two corners at the long sides of the room, equal surface area and view factor (to the operative temperature sensor) as with the dummies was achieved (see Figure 6). Correct surface area and view factor were essential in order to simulate mean radiant temperature and consequently the operative temperature. In the experiments, heat was transferred not only from the outside surface of the cylindrical thermal dummies but also

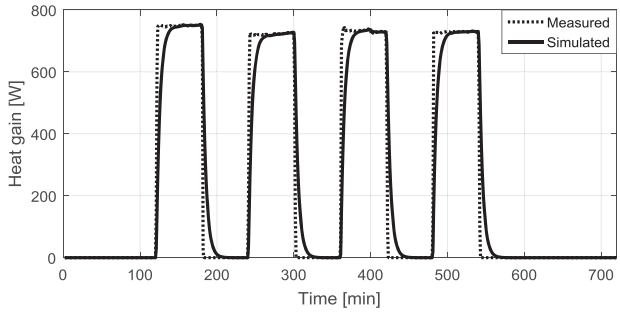

Figure 5. Measured and simulated internal heat gain in case 1.

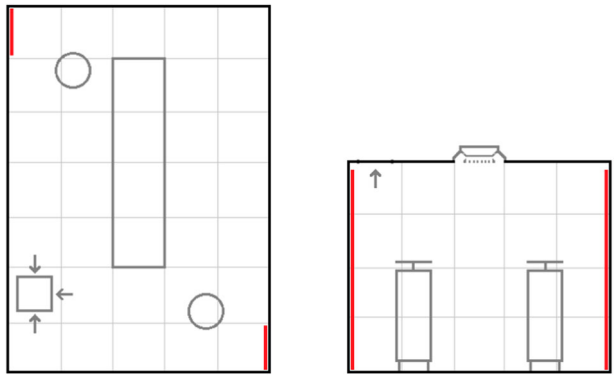

Figure 6. Declaration of how the heat gain was modelled. The thick red lines represent positioning of the flat electrical radiators.

from the inside surface (and from the lightbulbs). In the model, this was taken into account by allowing heat transfer on both sides of the flat radiators.

2.2.2. Active chilled beam

Filipsson et al. (2017) present an accurate thermal model of an ACB based on the NTU-effectiveness method. The model determines the cooling power as a function of the effectiveness, ε, the lower heat capacity rate, C_{min}, and the difference between room air, T_r, and chilled water supply temperature, $T_{w,in}$ (see Equation (11)).

$$P_w = \varepsilon \cdot C_{min} \cdot (T_r - T_{w,in}) \tag{11}$$

The heat capacity rate is determined by the flow rates of air or chilled water, while the effectiveness is determined by both flow rates as well as by the geometry of (heat transfer area) of the ACB. In the present study, flow rates of both air and chilled water are constant. Hence, Equation (11) may be relaxed and the ACB was modelled according to Equation (12) where k is an empirical constant.

$$P_w = k \cdot (T_{\boldsymbol{r}} - T_{w,in}) \tag{12}$$

2.2.3. Sensor corrections

To be able to compare results from the simulations with results from the measurements, the dynamic behaviour of the air and globe temperature sensors was taken into account. The sensors were exposed to a step-change in thermal climate from air and operative temperature of around 20°C to a climate of air and operative temperature of around 25°C. The time between the

Table 1. Convective heat transfer coefficients based on primary and supply air flow respectively (W/m^{2}K).

	Based on primary air flow	Based on supply air flow
Ceiling	7.9	18.8
Wall	2.5	6.6
Floor	2.3	5.1

step-change and a change in the value logged by the data acquisition system was used to determine the lag time (until the initial change) and the response time (until it reached 63% of the total change).

The lag times of both parameters were 2 min, the response time of the operative temperature was 4 min and the response time of the air temperature sensor was shorter than the sampling interval (1 min) and therefore not adjusted for.

2.2.4. Convective heat transfer coefficients

The CHTCs were modelled in accordance with Equations (8)–(10). In IDA ICE, the air change rate used in Equations (8)–(10) is determined by the primary air flow. In this study, simulations were made both with primary and supply air flow as determinant for the air change rate used in Equations (8)–(10). The primary air flow of 22.5 l/s means an air change rate of 2.68 ACH in the modelled room. The IR of the ACB used in this study was around five which implied a supply air flow of 135 l/s and a corresponding air change rate of 16.1 ACH. The air change rates used in this study implied that the BRIS model (Figure 2) was never applied. The CHTCs based on primary and supply air flow respectively are presented in Table 1.

2.2.5. Reference temperature

The heat transferred to the coil in an ACB is close to 100% convective. The validity of this assumption is supported by accurate and purely convective ACB models (Filipsson et al. 2017). However, the supply air discharged from the ACB, influenced by the Coandă effect, keeps the ceiling cold to a higher extent than generic convective cooling devices. This was taken into account by modelling the convective heat transfer at the ceiling as a function of the supply air temperature, i.e. assuming that the air temperature of Equation (1) equals the supply air temperature. This also implied that Equation (10) was replaced by Equation (4), which is valid under this assumption. The supply air temperature of an ACB is described by the following equation:

$$T_s = \frac{T_{pri} \cdot \dot{V}_{pri} + T_{sec,out} \cdot \dot{V}_{sec}}{\dot{V}_{pri} + \dot{V}_{sec}} \tag{13}$$

where T_{pri} and $\dot{V}_{pri}$ are the temperature and volumetric flow rate of the primary air, $\dot{V}_{sec}$ is the volumetric flow rate of secondary air and $T_{sec,out}$ is the temperature of the secondary air downstream the coil before mixing with the primary air.

The cooling capacity of the coil, P_w, generates a drop in the secondary air temperature according to the following equation where T_r is the room air temperature and ρ_a and $c_{p,a}$ are the density and specific heat capacity of air:

$$P_w = \dot{V}_{sec} \cdot \rho_a \cdot c_{p,a} \cdot (T_r - T_{sec,out}) \tag{14}$$

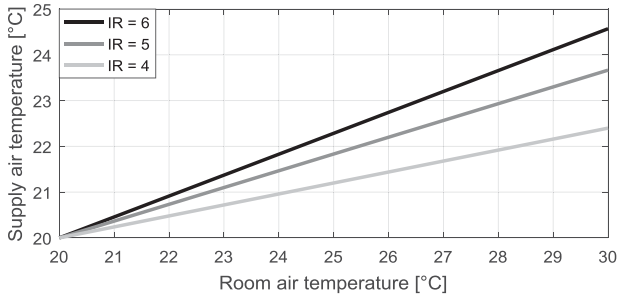

Figure 7. Supply air temperature as a function of room air temperature and IR.

The following equation defines the IR.

$$IR = \frac{\dot{V}_{sec}}{\dot{V}_{pri}} \tag{15}$$

Combining Equations (13)–(15) yields an expression for the supply air temperature, see the following equation:

$$T_s = \frac{T_{pri} + IR \cdot T_r - \frac{P_w}{\dot{V}_{pri} \cdot \rho_a \cdot c_{p,a}}}{1 + IR} \tag{16}$$

With the primary air and chilled water supply temperature used in this study (both 20°C) and a cooling coefficient of 76 W/K corresponding to the ACB used in this study (coefficient C in Equation (1)), the supply air temperature as a function of room air temperature and IR are according to Figure 7.

2.3. Whole year simulation

In order to estimate the consequences of erroneously simulated air and operative temperature, a more realistic simulation of an office room was carried out. The dimensions of the room were equal to the room in the previous model. One short side of the room was equipped with a window and exposed to the outdoor facing south while the other surfaces of the room were assumed adiabatically adjoined to other rooms. The room was equipped with a self-regulating ACB (constant flow of chilled water) dimensioned to not let the operative temperature in the room exceed 25°C for more than 80 h of occupancy annually. Additional parameters are presented in Table 2.

3. Results

3.1. Experiments and simulations

The measurements were compared to the results of different levels of adjustments to the original model, henceforth called models 1–3. The models are presented in Table 3.

As described in Section 2.1, two different cases with different levels of internal heat gain were performed. Around 58 W/m^2 in case 1 and around 38 W/m^2 in case 2. Figure 8 presents the measured and originally simulated air temperature in case 1. As seen in Figure 8, the simulated air temperature was more fluctuating than the measured. Since it was also generally lower than the measured, largest deviations are observed during the time when the heat gain was turned off.

Table 2. Input parameters to the model.

	Parameter	Value
External wall	Dimensions	3 × 2.4 m
	U-value	0.54 W/m^{2}K
Window	Dimensions	2.4 × 1 m
	U-value (incl. frame)	1.1 W/m^{2}K
	g-value	0.31
Primary air	Flow	22.5 l/s
	Temperature	20°C
	Schedule	07:00-19:00
Chilled water	Supply temperature	20°C at $T_{oa} > 20$°C, 22°C at $T_{oa} < -20$°C, linearly interpolated in between
	Schedule	07:00-19:00
Lighting/equipment	Power	15 W/m^2
	Schedule	Weekdays 08:00–17:00
	Radiative fraction	50%
Occupants	Quantity	1 person
	Schedule	Weekdays 08:00–12:00, 13:00–17:00
Outdoor climate		Stockholm, Sweden

Table 3. Description of the models.

Model	Description	
Model 0	Original unmodified model	
Model 1	Model 0 + Response time of sensors	As described in Section 2.2.3
Model 2	Model 1 + Adjusted CHTCs	As described in Section 2.2.4
Model 3	Model 2 + Supply air as reference temperature	As described in Section 2.2.5

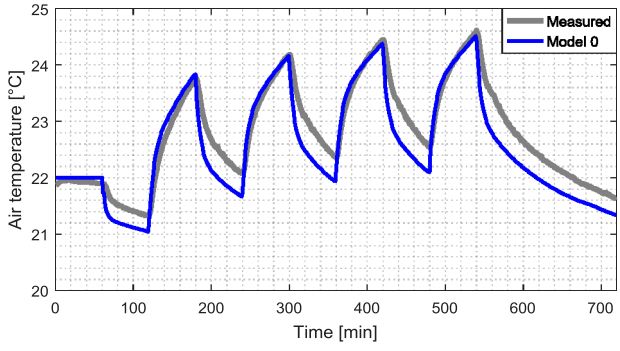

Figure 8. Measured and simulated room air temperature during case 1.

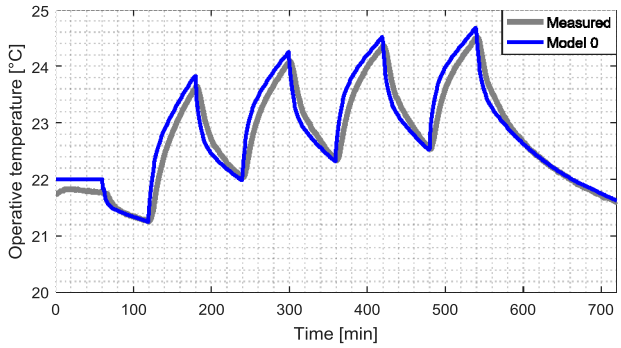

Figure 9. Measured and simulated operative temperature during case 1.

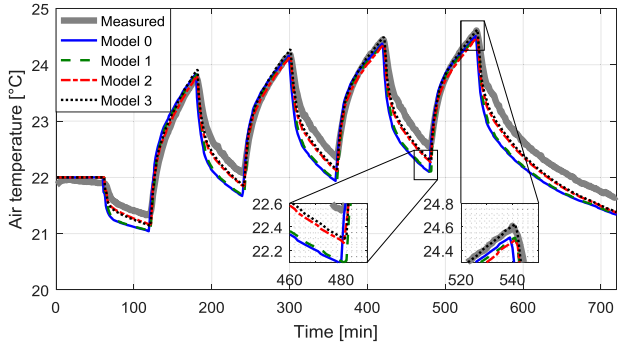

Figure 10. Room air temperature during case 1.

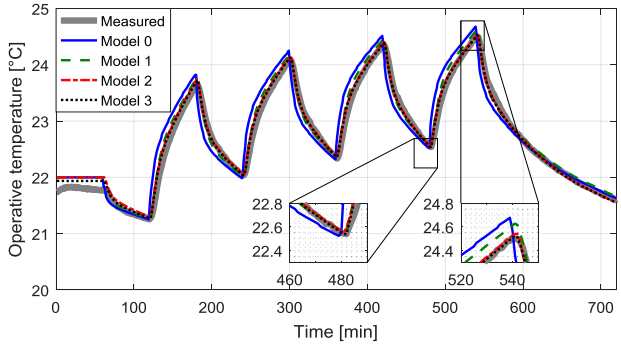

Figure 11. Operative temperature during case 1.

Figure 9 presents the measured and simulated operative temperatures. Similarly to the air temperature, the simulated operative temperature was lower than the measured one when the internal heat gain was turned off, but the opposite occurred when the internal heat gain was turned on.

In Figure 10, the air temperature simulated by all models is plotted to allow a comparison to the measured air temperature. In general, the simulations showed better correspondence during the peaks than during the troughs. Model 3 was closest to the measured value during both the peaks and the troughs.

All models showed better correspondence regarding operative temperature than regarding air temperature, (see Figure 11). The largest errors in operative temperature occurred at the warmest peak.

The results from case 2 were essentially the same as for case 1. Regarding the air temperature, model 3 was closest to the measured temperature at all times. This is presented in Figure 12.

The operative temperature differed less between the models. Models 2 and 3 showed approximately equally good correspondence to the measurements. This is presented in Figure 13.

In order to quantify the errors, the root-mean-square error was calculated according to the following equation where T_{sim} is the simulated and T_{mea} is the measured temperature at each minute i:

$$RMSE = \sqrt{\frac{1}{n}\sum_{i=o}^{n}(T_{sim,i} - T_{mea,i})^2} \quad (17)$$

All root-mean-square errors are presented in Figure 14.

Regarding air temperature, the major improvement was the adjustment of the CHTCs. Regarding operative temperature, the

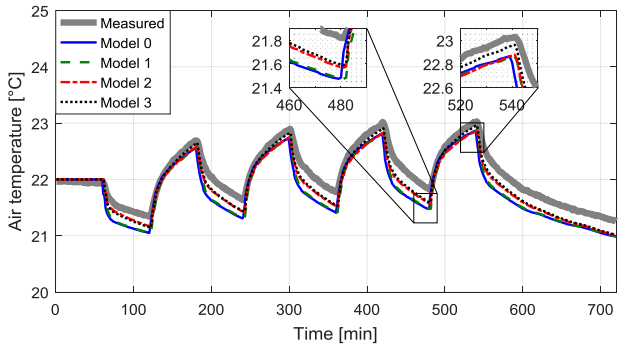

Figure 12. Room air temperature during case 2.

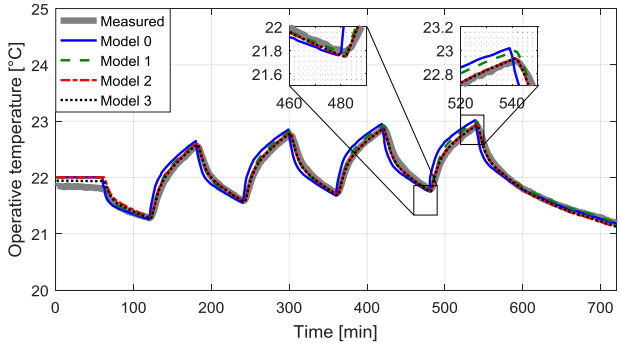

Figure 13. Operative temperature during case 2.

major improvement was taking the lag and response time of the sensors into account.

3.2. Whole year simulation

In this section, the simulations were not compared to any measurements and hence no lag and response time of sensors was taken into account. With the original unmodified model 0, a design cooling capacity of 394 W was required in order to not exceed an operative temperature of 25°C for more than 80 h of occupancy annually. The design cooling capacity was defined as the amount of heat transferred to the chilled water at a room air temperature of 25°C. In addition to determining the hours of occupancy with operative temperature above 25°C, it was also determined which design cooling capacity each model required in order to meet the design condition of maximum 80 h of operative temperature above 25°C. The results are presented in Table 4.

As seen in Table 4, in comparison to model 0, the results from model 3 showed 35% less hours of operative temperature above 25°C or, if the same design criterion is applied, a 9% lower design cooling capacity. Figure 15 shows the duration of

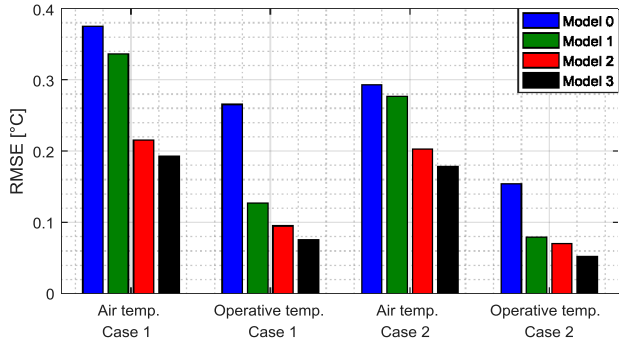

Figure 14. Root-mean-square errors of room air and operative temperature in all simulated models for both cases.

Table 4. Design cooling capacity and number of occupancy hours of operative temperature above 25°C.

	Design cooling capacity (W)	Time of $T_{op} > 25$ (h)
Model 0	394	80
Unchanged cooling capacity		
Model 2	394	56
Model 3	394	52
Unchanged design criterion		
Model 2	363	80
Model 3	358	80

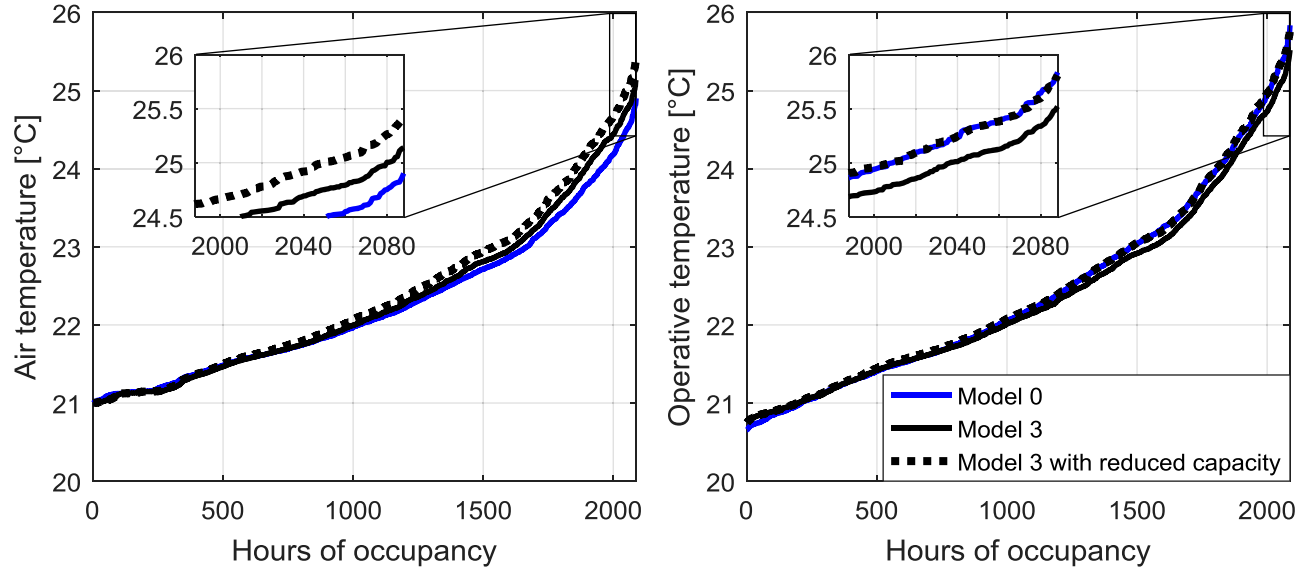

Figure 15. Duration of room air and operative temperature.

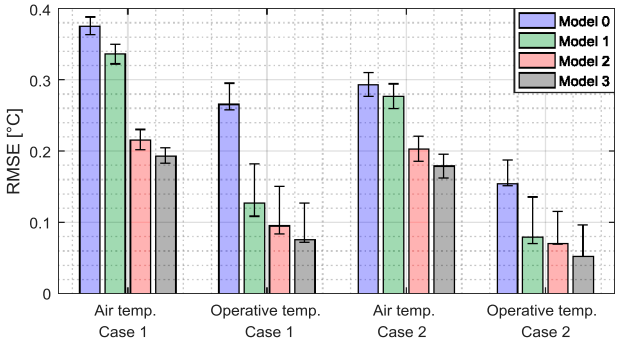

Figure 16. Uncertainty analysis of root-mean-square errors of room air and operative temperature in all simulated models for both cases.

air and operative temperatures for model 0 and model 3, with and without reduced cooling capacity. The lower operative temperature in model 3 is linked to higher air temperature. By using model 3 instead of model 0, the maximum operative temperature is reduced by 0.32°C while the maximum air temperature is increased by 0.24°C.

3.3. Measurement uncertainties

All measurements include uncertainties. This uncertainty analysis includes measurements of air and operative temperatures. The expanded uncertainties of the air temperature, globe temperature and air velocity were ±0.02°C, ±0.1°C and ±0.03 m/s respectively. For the operative temperature, this implies an expanded uncertainty of ±0.08°C. The error bars in Figure 16 show the corresponding RMSE taking these expanded uncertainties into account. Regarding the air temperatures, the upper end of the error bars always represents a situation where the actual temperature is higher than the measured and vice versa. Hence, the rank is not affected by the measurement uncertainties.

By contrast, the uncertainty of measured operative temperature is more influential. As seen in Figure 17, if the actual operative temperature was 0.08°C higher than the measured one, models 2 and 3 performed equally good in case 1, while model 1 performed better than the other models in case 2.

4. Discussion

There are several very accurate ACB models available. However, these focus on the cooling capacity. Correct simulation of the emitted cooling capacity, in terms of Watt, is not enough in order to obtain an accurate model of an ACB. In this paper, the IR and the relatively cold ceiling are taken into account in order to improve the accuracy of ACB modelling.

In a building performance simulation context, the accuracy is very good even without taking these features into account. The errors caused by this negligence are by far smaller than errors caused by erroneously predicted occupant behaviour, outdoor climate, thermal bridges, infiltration, etc.

However, that being said, the results presented in this study indicate that the accuracy of modelling ACBs improves when adjusting the CHTCs with respect to the IR and taking the relatively cold ceiling into account. If designing for a certain operative temperature, this will reduce the required design cooling capacity, i.e. reduce the required size of the ACB, reduce the required flow of chilled water and/or increase the required supply chilled water temperature. The reduced operative temperature is at the expense of a higher room air temperature. A higher room air temperature implies higher driving temperature difference further reducing the required design cooling capacity. If designing for a maximum allowed room air temperature, on the other hand, the adjustments presented in this study will imply a higher required cooling capacity.

The results presented in this study are applicable to ACB systems in general, but particularly relevant for high-temperature self-regulating ACBs. The self-regulation (constant flow of chilled water) means that there are no control valves and hence no compensation for the safety margins usually applied when designing the systems. The high-temperature chilled water, around or above 20°C, implies higher IR and a more distinct Coandă effect (as a consequence of the lower Archimedes number of the non-isothermal supply air jet). On the other hand, lower chilled water temperature gives a colder ceiling. But also, and above all, the high chilled water temperature implies a small driving temperature difference between the room air and the chilled

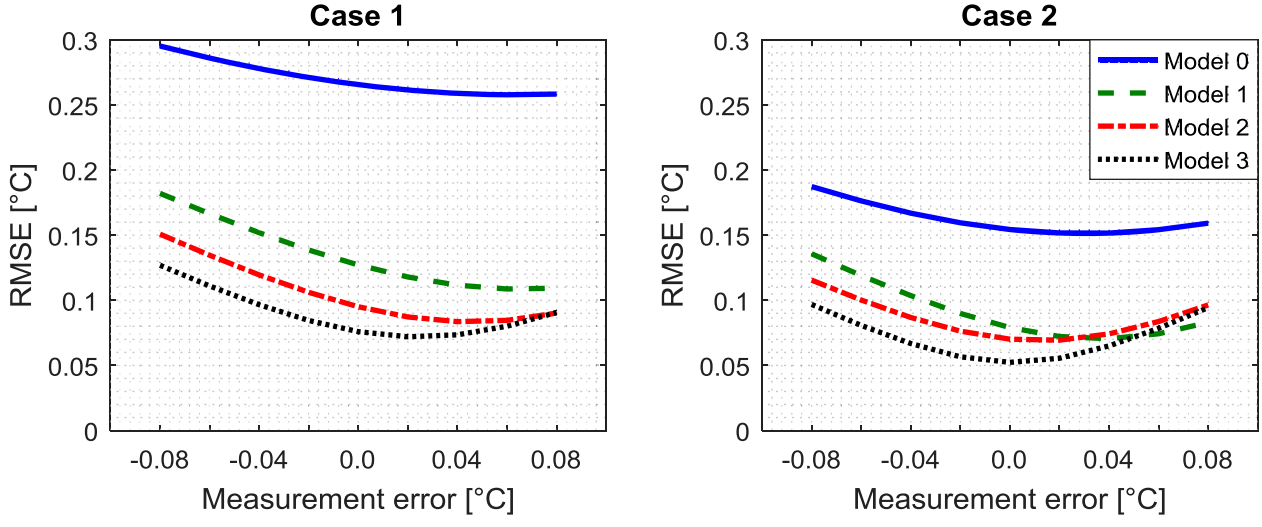

Figure 17. Uncertainty analysis of root-mean-square errors of operative temperature.

water. Consequently, a small error in simulated room air temperature has a large influence on the simulated required design cooling capacity. With conventional chilled water temperature (e.g. 14°C), the reduction in required design cooling capacity is substantially lower.

It shall be noted that the model used in this study is not undisputed and many other models are available. For example, Le Dréau, Heiselberg, and Jensen (2015) concluded that the CHTCs in rooms with ACBs were more accurately determined by taking the modified Archimedes number into account.

Developing CHTC models and finding the best correlations between known parameters and convective heat transfer require extensive measurements under numerous different circumstances. The purpose of the measurements presented in the present paper was neither to find such correlations nor to compare different existing models. Instead, only rough adjustments were made to a common implementation of one existing CHTC model to better represent a room with an ACB. The purpose of the measurements was to control how this influenced the model accuracy. Further studies are required in order to investigate whether the results from this study are applicable in a more general sense, regarding ACBs with different supply chilled water temperatures, different IRs, different air flow characteristics, and rooms with other geometries and differently positioned ACBs.

It can be noted, from Table 4, that the design cooling capacity is reduced. Accordingly, the size of the ACB may be reduced. However, this should not be confused with the actually obtained cooling capacity, which determines the design of the cooling source (e.g. the chiller) since the smaller ACB is compensated for by the higher room air temperature.

The cylindrical thermal dummies used for experiments were represented by flat heated surfaces in the model. Careful attention was paid in order to obtain the same surface area and angle factor between the flat surfaces and the sensor for operative temperature. However, this approach led to an inevitably erroneous angle factor between the heated surfaces and other surfaces in the model, e.g. the ACB and the walls.

Taking the chilled ceiling into account decreased the operative temperature. The fact that the higher CHTCs also decreased the operative temperature is not as obvious. The phenomenon is due to the fact that a relatively large part of the internal heat gain was radiative while the cooling was convective. In a room with more convective internal heat gain and/or more radiative cooling, higher CHTCs might lead to higher operative temperature.

5. Conclusions

ACBs have certain features that distinguish them from other cooling devices. Room air is induced, which affects the CHTCs of internal surfaces of the room, and they keep the ceiling cold to a greater extent than generic cooling devices. The results presented in this paper indicate improved accuracy of simulated indoor air and operative temperature when taking these features into account. In comparison to measurements, the RMSE of simulations of both air and operative temperature is reduced by 35–40%. In the studied design scenario with a chilled water supply temperature of 20°C, the proposed model met the design criterion at 9% lower required design cooling capacity.

Acknowledgements

This paper is a result of the research project *Self-Regulating Active Chilled Beam Systems*. The authors wish to thank Bengt Hellström at EQUA Simulation AB for his valuable support.

Disclosure statement

No potential conflict of interest was reported by the author(s).

Funding

The project is funded by the Construction Industry Organisation for Research and Development (SBUF) in Sweden (13426).

Nomenclature

k	empirical constant (W/K)
c_p	specific heat capacity (J/kgK)
P	cooling capacity (W)
h	convective heat transfer coefficient (W/m^{2}K)
q''	heat flux (W/m^2)
ρ	density (kg/m^3)
T	temperature (°C)
$\dot{V}$	volumetric flow rate (m^3/s)

Subscripts

a	air
conv	convection
in	inlet
mea	measured
oa	outdoor air
op	operative
out	outlet
pri	primary
r	room
s	supply
sec	secondary
sim	simulated
sur	surface
w	water

Abbreviations

ACB	active chilled beam
ACH	air changes per hour
CHTC	convective heat transfer coefficient
IR	induction ratio
NTU	number of transfer units
RMSE	root-mean-square error

ORCID

Peter Filipsson http://orcid.org/0000-0002-2385-0951
Jan-Olof Dalenbäck http://orcid.org/0000-0001-8771-0416

References

Cao, G., J. Kurnitski, P. Mustakallio, and O. Seppänen. 2008. "Active Chilled Beam Wall Jet Prediction by the Free Convection Model." *International Journal of Ventilation* 7 (2): 169–178.

CEN, European Committee for Standardization. 2008. "EN 15116 Ventilation in Buildings – Chilled Beams – Testing and Rating of Active Chilled Beams."âĂŃ

Chantrasrisalai, C., D. E. Fisher, I. Iu, and D. Eldridge. 2003. "Experimental Validation of Design Cooling Load Procedures: The Heat Balance Method." *ASHRAE Transactions* 109 (2): 160–173.

Chen, C., W. Cai, K. Giridharan, and Y. Wang. 2014. "A Hybrid Dynamic Modeling of Active Chilled Beam Terminal Unit." *Applied Energy* 128: 133–143.

DOE, Department of Energy, US. 2010. "Energyplus Engineering Reference: The Reference to Energyplus Calculations." https://energyplus.net/sites/default/files/pdfs_v8.3.0/EngineeringReference.pdf.

Domínguez-Muñoz, F., J. M. Cejudo-López, and A. Carrillo-Andrés. 2010. "Uncertainty in Peak Cooling Load Calculations." *Energy and Buildings* 42 (7): 1010–1018.

EQUA Simulation AB. 2010. "Validation of IDA Indoor Climate and Energy 4.0 Build 4 with Respect to ANSI/ASHRAE Standard 140-2004." http://www.equaonline.com/iceuser/validation/ASHRAE140-2004.pdf.

EQUA Simulation AB. 2018. "IDA Indoor Climate and Energy." Version 4.8 [Computer Software].

Filipsson, P., A. Trüschel, J. Gräslund, and J.-O. Dalenbäck. 2016. "Induction Ratio of Active Chilled Beams - Measurement Methods and Influencing Parameters." *Energy and Buildings* 129: 445–451.

Filipsson, P., A. Trüschel, J. Gräslund, and J.-O. Dalenbäck. 2017. "A Thermal Model of an Active Chilled Beam." *Energy and Buildings* 149: 83–90.

Filipsson, P., A. Trüschel, J. Gräslund, and J.-O. Dalenbäck. 2020. "Performance Evaluation of a Direct Ground-Coupled Self-Regulating Active Chilled Beam System." *Energy and Buildings* 209: 109691.

Fisher, D. E., and C. O. Pedersen. 1997. "Convective Heat Transfer in Building Energy and Thermal Load Calculations." *ASHRAE Transactions* 103: 137–148.

IEA. 2018. *The Future of Cooling - Opportunities for Energy-Efficient air Conditioning*. Paris: International Energy Agency.

ISO, International Organization for Standardization. 1998. "ISO 7726 Ergonomics of the Thermal Environment – Instruments for Measuring Physical Quantities."

Ji, K., W. Cai, X. Zhang, B. Wu, and X. Ou. 2019. "Modeling and Validation of an Active Chilled Beam Terminal Unit." *Journal of Building Engineering* 22: 161–170.

Kosonen, R., and F. Tan. 2005. "A Feasibility Study of a Ventilated Beam System in the Hot and Humid Climate: A Case-Study Approach." *Building and Environment* 40 (9): 1164–1173.

Le Dréau, J., P. Heiselberg, and R. L. Jensen. 2015. "Experimental Investigation of the Influence of the Air Jet Trajectory on Convective Heat Transfer in Buildings Equipped with Air-Based and Radiant Cooling Systems." *Journal of Building Performance Simulation* 8 (5): 312–325.

Livchak, A., and C. Lowell. 2012. "Don't Turn Active Beams into Expensive Diffusers." *ASHRAE Journal* 54 (4): 52–59.

Loutzenhiser, P., H. Manz, and G. Maxwell. 2007. "Empirical Validations of Shading/Daylighting/Load Interactions in Building Energy Simulation Tools: A Report for the International Energy Agency's SHC Task 34." ECBCS Annex, 43.

Maccarini, A., G. Hultmark, A. Vorre, A. Afshari, and N. C. Bergsøe. 2015. "Modeling of Active Beam Units with Modelica." *Building Simulation* 8 (5): 543–550.

Maccarini, A., M. Wetter, A. Afshari, G. Hultmark, N. C. Bergsøe, and A. Vorre. 2017. "Energy Saving Potential of a Two-Pipe System for Simultaneous Heating and Cooling of Office Buildings." *Energy and Buildings* 134: 234–247.

Mao, C., J. C. Baltazar, and J. S. Haberl. 2018. "Literature Review of Building Peak Cooling Load Methods in the United States." *Science and Technology for the Built Environment* 24 (3): 228–237.

Pedersen, C. O., D. E. Fisher, and R. J. Liesen. 1997. "Development of a Heat Balance Procedure for Calculating Cooling Loads." *ASHRAE Transactions* 103: 459–468.

Peeters, L., I. Beausoleil-Morrison, and A. Novoselac. 2011. "Internal Convective Heat Transfer Modeling: Critical Review and Discussion of Experimentally Derived Correlations." *Energy and Buildings* 43 (9): 2227–2239.

Wu, B., W. Cai, H. Chen, and K. Ji. 2018. "Experimental Investigation on Airflow Pattern for Active Chilled Beam System." *Energy and Buildings* 166: 438–449.